Effects of hypervelocity capture in aerogel on the compositions of iron–nickel-sulfide and feldspar minerals

S.M. Jones[1], N. Heinz[1]

[1]Jet Propulsion Laboratory, California Institute of Technology, Pasadena, California 91109-8099 (Steven.m.Jones@jpl.nasa.gov)

Introduction: The Stardust Mission spacecraft encountered the comet 81P/ Wild and collected dust from the comet in aerogel cells [1]. The Stardust sample return capsule containing the captured samples returned to earth in 2006. Since that time, some of the aerogel cells have been removed from the flight tray and cometary particles have been extracted from the aerogel. Analyses of the particles have determined that the particles are primarily olivine, pyroxenes, iron-nickel-sulfides, and metals, as well as some feldspars and GEMS (glass with embedded metal and sulfides) [2]. While many impact tests have been conducted to test the alterations that mineral grains may experience during hypervelocity capture in silica aerogel, many of the minerals found in the comet have not been tested. Also, many of the tests conducted were done with fairly large projectiles (>100 microns) and higher density silica aerogel. To better understand how hypervelocity impact capture can alter mineral grains, hypervelocity capture tests were conducted with 5 – 75 micron diameter iron-nickel-sulfide projectiles and with Stardust-like 10 – 50 mg/cc gradient density silica aerogel.

Experimental: Gradient density (10 – 50 mg/cc) silica aerogel was produced following production method developed for the Stardust Mission. Minerals were obtained from Minerals Unlimited and Mineralogical Research Co. The minerals used for these impact tests reported here were pentlandite, pyrite, troilite, pyrrhotite, millerite, albite, oglioclase, andesine and anorthite. Portions of each mineral were ground with a mortar and pestle and sieved (230 mesh). This resulted in powders with particles ranging from 5 microns to approximately 75 microns. Characterization of the mineral projectiles prior to impact tests was done with a Keyence HVX Digital Microscope, Horiba XGT – 7200 X-Ray Analytical Microscope, a Bruker Sentarra Raman Microscope and a Horiba LabRAM HR Evolution Raman Microscope (both utilizing (785 nm and 532 nm laser). The hypervelocity impact capture tests were done at the Ames Research Center Advanced Vertical Gun Range. The mineral powders were loaded into a metal carrier cup and launched at a target consisting of four 4 X 3 X 2 cm aerogel cells. Each impact test used a different mineral powder and aerogel cells. The powder dispersed during flight, forming a cloud of particles, most of which struck the aerogel cells. The range of the speeds of the projectiles over the eight shots done was from 5.23 to 5.70 km/s, approximating the 6.1 km/s capture speed of the cometary particles in the Stardust cometary collector.

Roughly fifty captured particles were manually extracted from the aerogel cells from each impact test. Most of the extracted particles included attached aerogel, although some of the particles were removed without any attached aerogel. The first three dozen of the particles extracted were placed between two round microscope cover slips that were taped together. These samples were used for Raman analysis. Additional particles were bonded to a microscope cover slip with a very thin layer of silicone sealant. These were used for X-ray fluorescence analysis, as well as Raman analysis when possible.

Results and Discussion: The results from the x-ray fluorescence analyses of the pentlandite and troilite particles, extracted from the aerogel after hypervelocity capture, are shown in Figures 1 and 2. The black-filled circles are the compositions of the as received mineral samples, while the unfilled circles are the compositions of the mineral projectiles after capture in the aerogel. Both types of these mineral projectiles lost sulfur as a result of the heating caused by the hypervelocity capture in aerogel. The varying amounts of sulfur loss is assumed to be correlated to the amount of heating experienced by the particles during capture [2, 3]. All of these extracted particles were found at the termini of capture tracks. The XRF results of captured mineral particles of pyrite, pyrrhotite and millerite showed similar losses of sulfur relative to the iron or nickel content, or both.

Figure 3 is the phase diagram obtained for the compositions of impact tested feldspar projectiles. The black-filled circles are the compositions of the as received mineral samples, while the unfilled circles are the compositions of the mineral projectiles after capture in the aerogel. The feldspar projectiles captured in aerogel all exhibited approximately the same elemental compositional as the untested projectiles, with possibly a slight loss in calcium relative to the amounts of sodium present.

Table 1 gives the results of the Raman analyses done on projectiles not used in the capture tests (sample standard peaks) and extracted impact tested projectile particles (experimental peaks). The pyrite particles extracted from the aerogel capture cells have Raman spectra very similar to that of the standard particles

and the Rruff data. It appears as though the surfaces of the pyrrhotite, troilite and pentlandite projectile particles were oxidized to hematite during the Raman analyses. There have been reports in the literature of iron being either oxidized or reduced during hypervelocity capture, depending on the capture conditions [4,5]. Hematite can be produced by the heating that is caused by the laser used to excite the sample in a Raman microscope [4,6]. The heating observed by Burchell, et al., [4,7] of various mineral particles during Raman analysis typically varied from 100C to 200C. Although, much higher temperatures were also reported, depending on the mineral. These temperatures are sufficient to convert iron on the surface of the iron bearing minerals to hematite in the presence of air. This oxidation during Raman analysis makes it difficult to obtain unambiguous Raman results of iron-nickel-sulfide samples. If the power of the Raman laser is reduced to try to prevent the oxidation reaction, then the signal to noise ratio of the spectra is low.

References: 1. Brownlee, et al., 2006 Science 314, 1711-1716. **2.** Zolensky, et al., 2006 Science, 314 1735-1739. **3**. Ishii, et al., 2008 LPSC Abstract 1561. **4**. Bridges, et al., 2010 MAPS, 45(1) 55-72. **5**. Stodolna, et al., 2013 Geochim. Cosmochim. Acta 122 1-16. **6**. Weber, et al., 2017 J. Raman Spec. 48 1509-1517. **7**. Burchell, et al., 2006 MAPS, 41(2) 217-232

Table 1 – Raman Spectroscopy Summary

Mineral	Chemical Formula	Experimental Peaks (Average, cm^{-1})	Sample Standard Peaks (Average, cm^{-1})	Rruff Database Peaks (Average, cm^{-1})
Pentlandite	$(Fe,Ni)_9 S_8$	218, 282, 387	216, 280, 392	243, 281
Pyrite	FeS_2	340, 367	338, 372	340, 375
Pyrrhotite	$Fe_{(1-x)}S$ (x = 0 to 0.2)	223, 288,405	220, 287, 398	322, 370
Troilite	FeS	220, 284, 394	217, 283, 402	203, 284, 396
Hematite				226, 293, 410

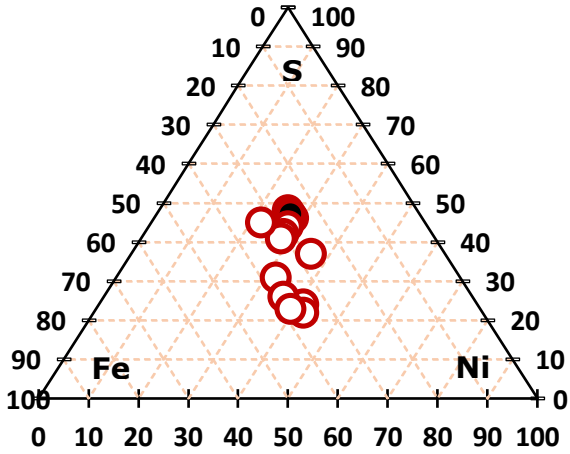

Figure 1 – Ternary phase diagram for pentlandite.

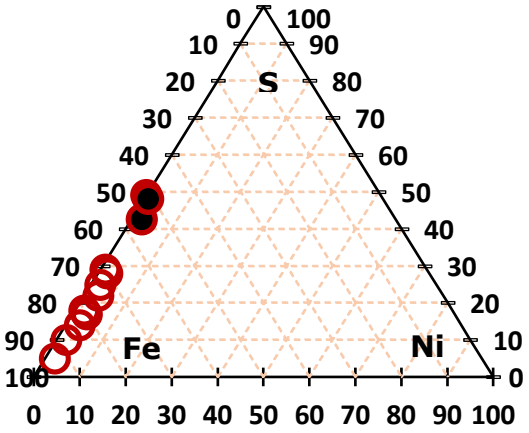

Figure 2 – Ternary phase diagram for troilite

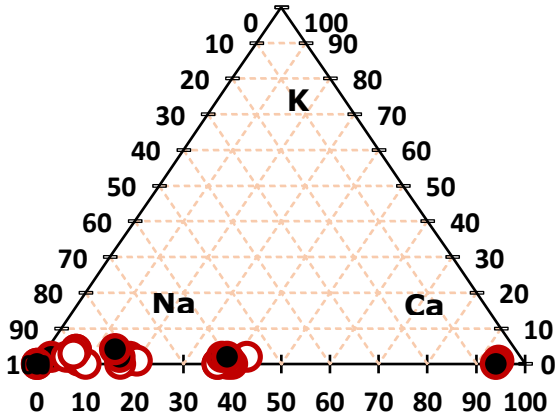

Figure 3 – Ternary phase diagram for feldspars.